Iranian Journal of Basic Medical Sciences
ijbms.mums.ac.ir

In silico and *in vivo* investigation of rotundic acid for its effect on cyclophosphamide-induced cardiotoxicity in Swiss albino mice; targeting TLR4/ NF-κB/ cleaved caspase-3

Mohammad Moonis [1], Mirza Sarwer Baig [2], Divya Vohora [1], Syed Ehtaishamul Haque [1]*

[1] Department of Pharmacology, School of Pharmaceutical Education and Research (SPER), Jamia Hamdard, New Delhi–110062, India
[2] Centre for Virology, School of Interdisciplinary Sciences & Technology (SIST), Jamia Hamdard, New Delhi–110062, India

ARTICLE INFO

Article type:
Original

Article history:
Received: Apr 25, 2025
Accepted: Nov 25, 2025

Keywords:
Cyclophosphamide
Cardiotoxicity
Cardiac inflammation
Cancer
Cardiac fibrosis
Oxidative stress
Rotundic acid
Swiss albino mice

ABSTRACT

Objective(s): To investigate rotundic acid (RA), a triterpenoid, for its protective role against the cyclophosphamide (CP) induced cardiotoxicity in Swiss albino mice, as CP, although a potent anticancer drug, induces severe cardiotoxicity as a side effect in cancer patients. Thus, this study was a step towards developing an adjuvant that can reduce the toxicity of CP during cancer treatment.

Materials and Methods: Animals were randomly assigned to 7 groups. Control; CP 200; RA 10 + CP 200; RA 20 + CP 200; RA 40 + CP 200; NER 400 + CP 200 and RA 40 *perse*. RA was given orally for 14 days, and CP 200 mg/kg, IP, once on the 7th day. On the 15th day, animals were sacrificed, and blood and heart samples were collected for investigations.

Results: CP 200 mg/kg, IP, enhanced the level of cardiac troponin T, CK-MB, LDH, NF-κB, TLR4, TNF-α, IL-6, IL-Iβ, cleaved caspase-3, TBARS, nitrite, and reduced the level of CAT, GSH, and SOD, resulting in cardiac injury, nitrative stress, oxidative stress, inflammation, and fibrosis. Administration of RA and nerolidol substantially reversed these pathological modifications to normal. Molecular docking study showed that RA strongly binds to the pocket domains of TLR-4 and cleaves caspase-3.

Conclusion: The findings suggest that RA has the potential to reduce the toxicity of CP in the heart and can be utilized as an additional treatment for cancer therapy, along with CP. However, further research using animal models for cancer is required to confirm this.

▶ Please cite this article as:
Moonis M, Sarwer Baig M, Vohora D, Haque SE. *In silico* and *in vivo* investigation of rotundic acid for its effect on cyclophosphamide-induced cardiotoxicity in Swiss albino mice; targeting TLR4/ NF-κB/ cleaved caspase-3. Iran J Basic Med Sci 2026; 29: 401-411. doi: https://dx.doi.org/10.22038/ijbms.2026.87759.18960

Introduction

Cyclophosphamide (CP), an alkylating agent, is widely used as an anticancer and immunosuppressive drug (1). Despite its potent anti-cancer effects, high dose of CP is not used for the treatment of cancer due to its various side effects, such as cardiotoxicity, which are caused mainly by oxidative stress (2). CP is rapidly metabolized in the liver by cytochrome P450 enzyme and converted into phosphoramide mustard (PM), aldophosphamide, 4-hydro-cyclophosphamide, and acrolein (3). PM is an anticancer moiety that disrupts the N-7 guanine residues of DNA to kill cancerous cells, and acrolein is responsible for cardiotoxicity by disrupting the anti-oxidant system through the generation of superoxide radicals and hydrogen peroxide (4). The Reactive Oxygen Species (ROS) so generated damage the inner mitochondrial membrane of the heart and reduce its activity and overall function (5). Cardiotoxicity is driven by persistent overproduction of reactive oxygen and nitrogen species (ROS and RNS), depletion of endogenous anti-oxidant enzymes, enhanced lipid peroxidation (TBARS), and elevation of cardiac injury biomarkers (CK-MB, cTnT, LDH). Apoptotic cell death is further evidenced by increased cytochrome c release and up-regulated cleaved caspase-3 expression. Additionally, CP triggers inflammatory and fibrotic responses through modulation of Nrf2, NLRP3 inflammasome, TGF-β1, NF-κB, and p38 MAPK pathways activation (6).

At present, there is no established therapeutic strategy to counteract CP-induced cardiotoxicity. The co-administration of agents capable of attenuating CP-mediated toxicity represents a potential approach for cardio protection. Natural bioactive compounds are increasingly investigated for their pharmacological efficacy as they are safe, efficient, and economical (7). We selected rotundic acid (RA) to investigate its cardioprotective potential against CP-induced cardiotoxicity because it is a pentacyclic triterpenoid, a bioactive compound found in the plant "Jiubiying" (8), and has several pharmacological properties, including anti-oxidant, anti-inflammatory, anti-cancer, antidiabetic, and antibacterial (9). It shows anti-inflammatory activity by inhibiting various markers such as IL-6, TNF-α, COX-2, and iNOS (10) RA down-regulate various pathways like PI3K, MAPK, and NF-κB, and up-regulate Nrf2 signaling pathway (11). A study also showed that RA alleviates inflammation and adipogenesis in nonalcoholic steatohepatitis (NASH)

***Corresponding author:** Syed Ehtaishamul Haque. Department of Pharmacology, SPER, Jamia Hamdard New Delhi, India – 110062. Email: sehaq@jamiahamdard.ac.ir

by suppressing glycolysis and lactate production, besides attenuating inflammation through modulation of the TLR4/AP1 signaling pathway (12). However, there is no single study available that shows RA protects against CP-induced cardiotoxicity. Therefore, we decided to evaluate the protective effect of RA against CP-induced cardiotoxicity in Swiss albino mice.

Nerolidol (NER), an acyclic sesquiterpene, is widely used in food, cosmetics, and non-cosmetic industries (13). It is used as a fragrance agent in shampoo and detergents, and improves skin penetration. It has been reported to cause cytoprotective effects by activating anti-oxidant signaling pathways and decreasing inflammatory and apoptotic signaling pathways (14). Currently, it has been reported that nerolidol reduces oxidative stress, inflammation, fibrosis, and apoptosis against CP-induced cardiotoxicity in a mouse model (15).

Materials and Methods

Experimental animals

Swiss albino mice (25–35 g) were acquired from the Central Animal House Facility (Jamia Hamdard, New Delhi) after ethical approval from the Institutional Animal Ethics Committee (IAEC) with Proposal No. 2084. Animals were kept in standard conditions (12 hr light and dark cycle, temperature (23 ± 2 °C), humidity (60% ± 5%)) and were fed a pellet diet and water *ad libitum*.

Chemicals

Cyclophosphamide, Rotundic acid, ELISA kits (interleukins, cTnT), antibodies for TLR4, NF-kB, and Caspase-3 were procured from Sigma–Aldrich, ELK Biotechnology USA, and Krishgen Biosystems, Worli, Mumbai, India. The remaining chemicals and reagents used were of analytical grade.

Treatment regimen

Albino mice (42) were separated into seven groups (n=6). Group I- Control; treated with normal saline. Group II-Toxic; treated with CP 200 mg/kg, *IP* (16); Group III, IV & V; treated with rotundic acid 10, 20, and 40 mg/kg/oral, respectively (17, 18). Group VI- *Perse*; treated with rotundic acid 40 mg/kg /oral. Group VII- Standard; treated with NER 400 mg/kg/oral (3). Animals were treated with CP once on the 7th day and RA and NER for 14 days. On the 15th day, mice were euthanized by using CO_2 inhalation, sacrificed, and blood and heart samples were collected. The heart was stored in a 10% formalin solution for performing biochemical, histopathological, and immunohistochemical analysis. The entire treatment plan is shown in Figure 1.

Molecular docking

Preparation of ligands and proteins

The most dependable Protein Data Bank (Rutgers University, USA) hosted by the RCSB was used to download Toll-like receptor 4 (TLR4, PDB ID-2Z64), a protein of *Mus musculus*. The PyMol (19) Program was used to analyze protein structures retrieved from the PDB. The AlphaFold service was used for proteins whose crystallographic or NMR structures were not available in RCSB-PDB or other publicly accessible structural databases. The AlphaFold server was used to model protein caspase-3, which was 277 amino acids long. In the Swiss-Pdb viewer (version 4.1.0), the bonded atoms, dihedral angles, and torsions of the protein backbone, as well as the side chains, were further tuned for the protein structures (20). The triterpenoid ligand, Rotundic Acid (PubChem ID- 12315075), was retrieved in 2D (SDF) format from PubChem (https://pubchem.ncbi.nlm.nih.gov/) (Figure 2). Subsequently, the downloaded SDF file of the ligand was converted to 3D formats (.mol2 and .pdb) using ChemOffice 2016. Rotundic acid is a naturally occurring compound found in *Ilex chinensis*, *Ilex excelsa*, and various other organisms.

Molecular docking procedure

The process of molecular docking was executed utilizing the Auto Dock Vina tool (21). At first, the protein structures obtained from the RCSB-PDB were prepared by removing heteroatoms, previously docked ligands, and H_2O molecules. Following this step, polar hydrogen (H_2) atoms were introduced to the protein structures, which were either modeled by AlphaFold or sourced from PDB. Integration of Kollman charges (partial) was performed, ensuring that any charge deficit was evenly spread among all atoms in the protein residues. Subsequently, the charged and hydrogenated (polar only) protein structures in pdb files were converted into the pdbqt format with the aid of AutoDock Tool (version 1.5.7) (22). Grid boxes of various dimensions in X-, Y-, and Z- axes were established for

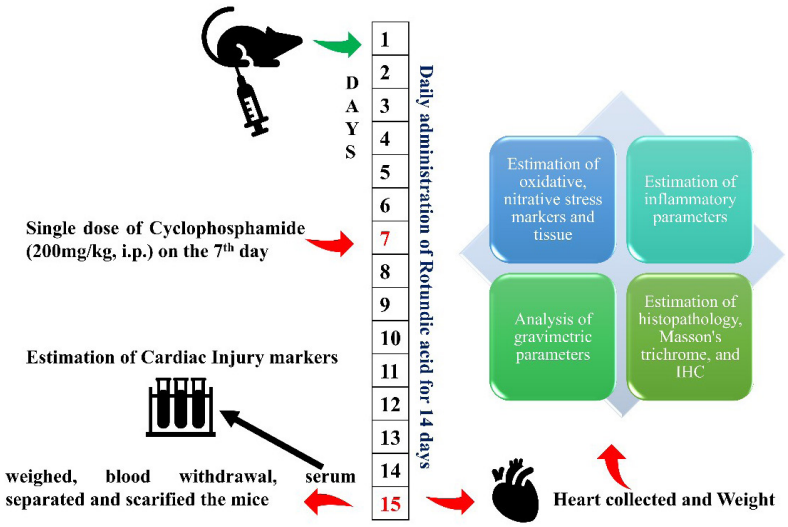

Figure 1. Design of the experimental procedure of the study

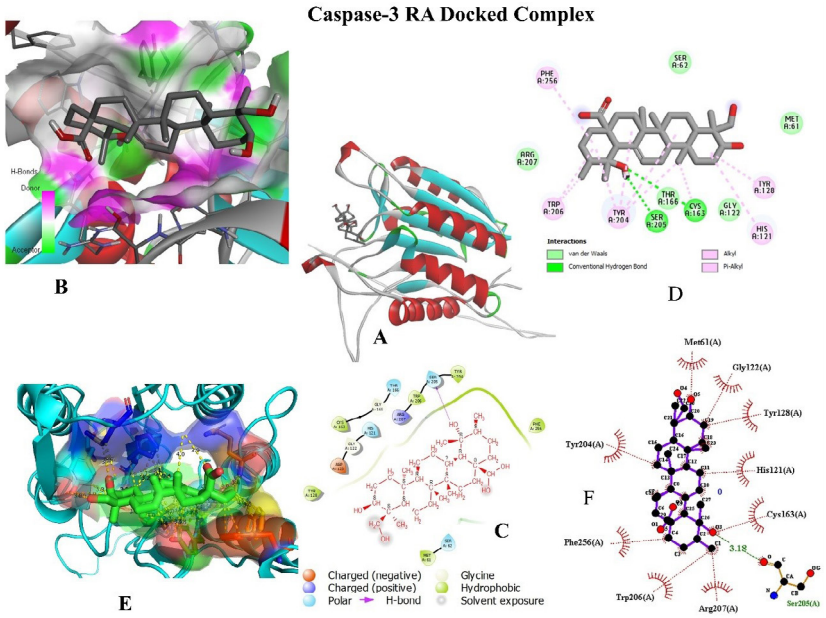

Figure 2. (A) A Discovery Studio diagram of rotundic acid (RA) docked with caspase-3. (B) RA binds within a cavity of caspase-3 that contains both hydrophilic and hydrophobic amino acids. (C) A magnified view of the caspase-3 binding cavity, showing the hydrophobic, charged, polar, glycine, and solvent-exposed amino acids. (D) A 2D graph showing the interactions between RA and the caspase-3 binding cavity at the molecular level. (E) A 3D PyMol image showing the interactions (yellow broken lines) of RA (green sticks) with the binding residues of caspase-3 (cyan and rainbow colors). (F) A LigPlot+ image showing the atomic-level hydrogen and van der Waals interactions between RA and the binding cavity residues.

different PDB proteins using ADT version 1.5.7 (Table 1). A grid box with dimensions of X = 102, Y = 74, and Z = 72 was generated for TLR4 and X = 88, Y = 58, and Z = 80 was drawn for cleaved caspase-3 to define the area for small-molecule docking (23–25). Moreover, the ligand molecule, rotundic Acid (Pub Chem ID-12315075), in pdb format, underwent Gasteiger-Marsili partial charging before being transformed into pdbqt format. The assessment of free energy (ΔG) involved analyzing intra-molecular hydrogen bonds, hydrophobic, ionic, and Van der Waals (vdW) interactions within the protein-ligand complexes to determine the binding affinity.

Evaluation of oxidative stress markers

Assessment of superoxide dismutase (SOD) activity

SOD activity was evaluated by using the method of Marklund (1974). This method relies on the ability of the SOD enzyme to inhibit pyrogallol (autoxidation). 10 µl of supernatant with Tris-HCl buffer was mixed, and the volume was increased to 3 ml by adding more Tris-HCl. Next, 25 µl pyrogallol was added to the mixture, and a spectrophotometer was used to examine the change in absorbance at 420 nm. Based on this method, one unit of SOD is defined as the quantity of SOD enzyme that inhibits 50 % of pyrogallol autoxidation per minute (26).

Assessment of catalase activity (CAT)

The procedure (Claiborne, 1985) of mixing 10 µl of cytosolic supernatant with phosphate buffer solution and hydrogen peroxide (H_2O_2) was used to analyze this. The rate of H_2O_2 disappearance was determined using a spectrophotometer at 240 nm. The disappearance rate was measured in nano moles of H_2O_2 / min/mg protein (27).

Assessment of reduced glutathione (GSH) activity

GSH was determined using the method of Sedlak and Lindsay (1968). To prepare the cytosolic supernatant, 10 µl was added to the EDTA and TCA mixture. The mixture was again mixed with Tris buffer and 5,5-dithiobisnitrobenzoic acid (DTNB), then, within 5 min, the absorbance was measured at 412 nm (28).

Assessment of lipid peroxidation

This test was performed using the technique described by Ohkawa *et al.* in 1979. The technique was utilized to quantify malondialdehyde (MDA). The tissue was homogenized, mixed with both thiobarbituric acid (TBA) and trichloroacetic acid (TCA). The solution was heated to 80 °C in a water bath, then cooled. Absorbance was measured at 540 nm (29).

Inflammatory and cardiac markers

LDH and CK-MB markers were estimated in serum by using commercially available kits following the manufacturer's instructions. They were purchased from Arkray Healthcare (Mumbai) and Reckon Diagnostics, India. cT-nT was bought from Krishgen Biosystems (India), and inflammatory parameters (IL-6, IL-1β, TNF-α) were

Table 1. Binding energies of rotundic acid and the standard drug nerolidol (Pub Chem-ID- 5284507) to TLR4 and caspase-3 proteins, as determined by auto Dock vina

S. No	Protein name (RCBS-PDB ID or alpha fold)	Name of chains	Grid points in X, Y, & Z dimensions	Binding energy (ΔG) (kcal/mol) of rotundic acid	Binding energy (ΔG) (kcal/mol) of standard nerolidol	No. of hydrogen bonds	Hydrogen bond forming residues
1.	TLR4 (2Z64)	A, C	102, 74, 72	-7.8	-5.9	2	ARG^{90}, GLU^{92}
2.	Cleaved caspase-3 (Alpha fold)	A	88, 58, 80	-8.0	-5.4	2	SER^{105}, CYS^{163}

ARG: arginine; GLU: glutamine; SER: serine; CYS: cysteine

purchased from ELK Biotechnology, USA.

Estimation of nitric oxide (NO)

Accumulation of nitrite concentration in cardiac tissue indicates the generation of nitric oxide (NO). NO was quantified using the Griess reagent, which consists of naphthyl ethylenediamine di-hydrochloride (0.1%), phosphoric acid (5%), and sulfanilamide (1%). Equal volumes of Griess reagent and supernatant were mixed and heated at room temperature for 10 min. The absorbance was taken at 520 nm (30).

Estimation of gravimetric parameters

The mice were weighed twenty-four hours after the final dosage. The animals were killed, their hearts were extracted, and thoroughly cleansed using a 0.9% solution of normal saline. Then the hearts were dehydrated with the help of filter paper and weighed to assess the ratio of heart weight (HW) to body weight (BW) (31).

Estimation of histopathology and immunohistochemistry (IHC)

After removal, the tissue was preserved in 10% formalin, cut, and embedded in paraffin wax for immunohistochemical (IHC) and histopathological analysis (H&E and MT). Transverse slices measuring five µm were applied for histopathology and IHC evaluation (32). The application of (H&E) dye was used to stain and analyze pathological alterations. The approach of reciprocal intensity analysis using Fiji (ImageJ) software was used to analyze semi-quantitative protein expression. For immunohistochemistry, heart tissue slices were treated with xylene to remove paraffin. Subsequently, a series of ethanol solutions of increasing concentration was used to dehydrate the tissue. Purified water obtained by a process of double distillation was used for the purpose of washing, and further steps were carried out accordingly (32). The computerized motic microscope, was used to capture the pictures.

Statistical analysis and data representation

The data are displayed as the mean ± SEM for each set of six mice. An analysis by ANOVA (one-way) with Tukey's test was employed to ascertain the significance between various groups. GraphPad Prism (version 5.01) was used, and $P<0.05$ was considered significant. "Effect sizes" with 95% confidence intervals (CI) were provided to ensure clarity and reliability of the findings.

Results

Molecular Docking of TLR4 and caspase-3

In our molecular docking analysis, we observed the interactions between RA and various proteins, shedding light on the extent of their binding affinities. The binding energies of RA and the standard drug NER with TLR4 and caspase-3 were determined using the Auto Dock Vina tool. Table 1 shows the protein name, its PDB ID or AlphaFold designation, the names of the chains involved, the binding Energy (ΔG) in kcal/mol for both RA and NER, the number of hydrogen bonds, and the residues involved in hydrogen bond formation. TLR4 with chains C showed binding energies of -7.8 kcal/mol for RA and -5.9 kcal/mol for NER, where the TLR4 binding cavity forms two hydrogen bonds through ARG^{90} and GLU^{92} residues. Alpha Fold modeled caspase-3 having single chain A displayed binding energies of -8.0 kcal/mol for RA and -5.4 kcal/mol for NER. Caspase-3 binding residues- SER^{205} and CYS^{163}- also form 2 hydrogen bonds with our drugs. When docking RA with caspase-3, as depicted in the Discovery Studio diagram (Figure 2), RA effectively bound within a distinct cavity of caspase-3, rich in both hydrophilic and hydrophobic amino acids (Figure 2A, 2B). A closer examination of this binding site (Figure 2C) revealed the presence of hydrophobic, charged, polar, glycine, and solvent-exposed amino acids. The 2D interaction graph (Figure 2D) delves into the molecular-level interactions, where hydrogen bonds with SER^{205} and CYS^{163}, along with several interactions with amino acids like SER^{62}, THR^{166}, ARG^{207}, MET^{61}, and GLY^{122}, were identified. Additionally, Alkyl and Pi-Alkyl bonds were observed between RA and THR^{128}, HIS^{121}, THR^{204}, TRP^{206}, and PHE^{256}. The 3D visualization using PyMol (Figure 2E) showcases these interactions, highlighting the intricate bonding patterns (yellow broken lines) between RA (green sticks) and caspase-3 binding residues (cyan and rainbow colors). The LigPlot+ image (Figure 2F) portrays further details of atomic-level interactions, displaying hydrogen bonds with SER^{205} and numerous hydrophobic interactions with amino acids like SER^{62}, THR^{128}, HIS^{121}, THR^{204}, TRP^{206}, PHE^{256}, THR^{166}, ARG^{207}, MET^{61}, and GLY^{122}. These findings offer crucial insights into how RA interacts with the binding cavity of caspase-3, providing valuable information for potential therapeutic applications.

For further insight, the molecular docking of RA with the Alpha Folded TLR4 binding sites was performed (Figure 3). Within this context, RA was found in a cavity composed of amino acid residues of C-chain serving as H-bond donors (pink) and acceptors (green) (Figure 3B). A detailed view of the TLR4 binding cavity highlights the characteristics of the exposed amino acids, encompassing hydrophobic, charged, and polar properties (Figure 3C). The molecular interactions between RA and the TLR4 binding cavities are comprehensively presented through a 2D graph generated using Discovery Studio software (Figure 3D). In this analysis, several amino acids, including PHE^{76}, LEU^{78}, LEU^{94}, PHE^{119}, and GLU^{122}, engaged in Van der Waals (VDW) interactions. Notably, two hydrogen bond-forming residues, ARG^{90} and GLU^{92}, have been identified. Additionally, RA forms alkyl and pi-sigma bonds with specific residues. For a three-dimensional perspective on the interactions between RA and TLR4-binding residues, a PyMol surface image is featured (Figure 3E). Furthermore, a LigPlot+ image (Figure 9F) provides a detailed representation of hydrophobic contacts (ILE^{46}, VAL^{61}, PHE^{76}, LEU^{78}, GLU^{92}, LEU^{94}, PHE^{104}, ILE^{117}, and PHE^{121}) and the atomic-level formation of hydrogen bonds (ARG^{90}) between RA and the binding cavity residues.

Assessment of RA via gravimetric parameter

Table 2 shows the weights of the heart (HW) and body (BW), as well as the HW/BW ratios for various groups. After CP 200 administration, heart weight of the CP 200-treated group significantly increased as compared to the control group ($P<0.001$). In contrast, all treated groups (RA 10, 20, 40, and NER 400) exhibited a non-significant increase compared to the CP 200 toxic group ($P>0.05$). The measurement of BW showed a pattern similar to that of heart weight. The ratio of HW/BW enhanced significantly in the CP 200 group, compared to the control group ($P<0.001$). RA 20, 40, and NER 400 significantly reduced the HW/BW ratio compared with the CP 200 toxic group

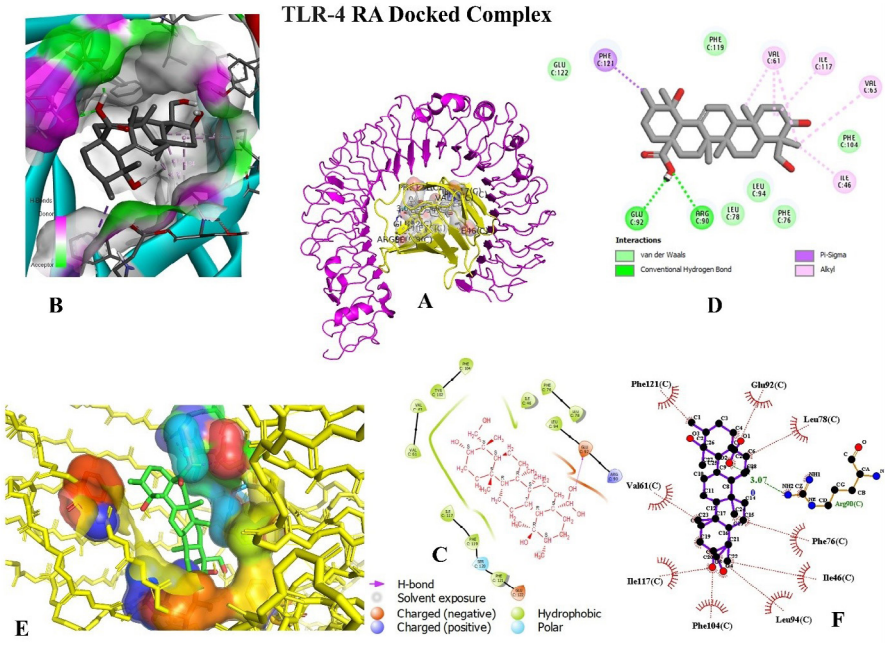

Figure 3. Showing *in silico* studies with TLR4
(A) Rotundic acid (RA) docked with the Alpha Folded TLR4 binding site's C-chain. (B) A cavity containing the amino acid residues of the H-bond donor (pink) and acceptor (green) is where RA is docked. (C) A close-up of the TLR4 binding cavity that emphasizes the amino acids that are exposed to solvent, hydrophobic, charged, and polar. (D) The molecular interactions between RA and the TLR4 binding cavity are shown in a Discovery Studio 2D graph. Amino acids such as PHE76, LEU78, LEU94, PHE119, and GLU122 generate VDW interactions, and two hydrogen bond-forming residues, ARG90 and GLU92, have been identified. Remarkably, RA and residues can also form alkyl and pi-sigma bonds. (E) A three-dimensional PyMol surface image showing interactions between RA and TLR4 binding residues. (F) A LigPlot+ image renders the hydrophobic contacts (ILE46, VAL61, PHE76, LEU78, GLU92, LEU94, PHE104, ILE117, and PHE121) and atomic-level hydrogen bond formation (ARG90) between RA and the binding cavity residues more clearly.

Table 2. The effect of rotundic acid (RA) on gravimetric parameters in Swiss albino mice

Groups	Body weight (g)	Heart weight (mg)	Heart and body weight ratio (mg/g)
Normal control	31.5 ± 0.364	188 ± 1.60	6 ± 0.09
CP 200	28.0 ± 0.587$^{###}$	196 ± 1.08$^{###}$	7 ± 0.2$^{###}$
RA10 + CP 200	28.0 ± 0.635^{ns}	194 ± 0.953^{ns}	7 ± 0.1^{ns}
RA 20 + CP 200	29.3 ± 0.358^{ns}	191 ± 1.17^{ns}	7 ± 0.08*
RA 40 + CP 200	30.2 ± 0.465*	189 ± 1.36**	6 ± 0.09***
NER 400 + CP 200	30.5 ± 0.377**	189 ± 0.785**	6 ± 0.08***
RA *Perse*	31.3 ± 0.287	189 ± 0.385	6 ± 0.06

Data are shown in table as mean ± SEM (n=6), data significance were assessed through ANOVA (one-way) with Tukey's test and ### P<0.001 data shown significant changes versus control, ns P>0.05 showed non-significant changes vs CP 200, * P<0.05,** P<0.01, and *** P<0.001 displayed significant changes vs CP 200.

(P<0.01, P<0.001). However, RA 10 showed no significant differences from the CP 200 group (P>0.05).

Assessment of RA via nitrative (NO) and oxidative stress markers

In cardiac tissue, CP 200 significantly lowered anti-oxidant markers (SOD, CAT, and GSH) and increased TBARS and nitrite levels as contrasted to normal control (P<0.001). The RA10 showed a non-significant effect on CAT, SOD, GSH, TBARS, or nitrite (P>0.05). RA 20, 40, and NER 400 considerably increased CAT, SOD, GSH and reduced TBARS, and nitrite levels in cardiac tissues (P<0.05, P<0.01, P<0.001) contrasted to the CP 200 group. There were no significant changes found in the RA *Perse* group as compared to the normal control (Figure 4).

Assessment of RA via cardiac damage markers

CP 200 showed significantly increased LDH, CK-MB, and cTn-T levels when compared with the normal control (P<0.001). The RA 10 administered group showed no significant decrease in these parameters. However, RA 20, 40, and NER 400 significantly reduced the levels of CK-MB, LDH, and cTn-T when compared with CP 200 (P<0.05, P<0.01, and P<0.001, respectively). RA *perse* did not show any alteration when compared with the normal control (Figure 5).

Assessment of RA via inflammatory markers

The CP 200 group showed significantly higher levels of inflammatory markers (interleukin-1β, IL-6, and TNF-α) than the normal control (P<0.001). RA 20, RA 40, and NER 400 significantly reduced these inflammatory markers in heart tissues as compared to CP 200 (P<0.01, P<0.001, and P<0.001, respectively). However, RA10 did not show any considerable changes (P>0.05). The study found that RA *perse* alone had no impact on these markers when contrasted to normal control (Figure 6).

Assessment of RA through immunohistochemistry (IHC) of NF-κB, TLR4, and cleaved caspase-3

CP 200 significantly elevated cleaved caspase-3, TLR4, and NF-κB expression in heart tissues (P<0.001). RA10 had no significant effect on these expressions (P>0.05). However, RA 20, 40, and NER 400 significantly decreased the expression of cleaved caspase-3, NF-κB, and TLR4 (P<0.001). RA *perse* has shown no significant changes as compared to the control (Figures 7, 8, 9, and 12).

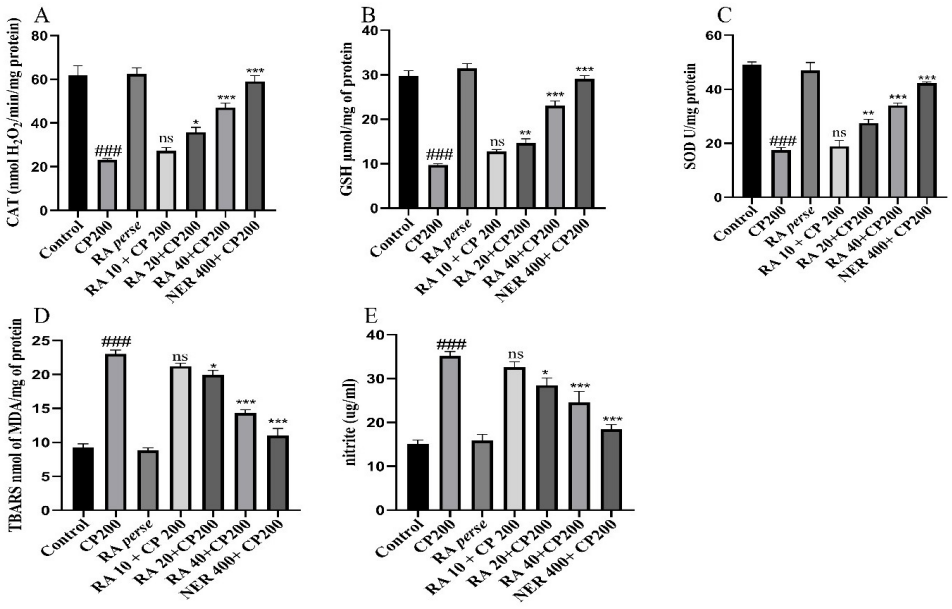

Figure 4. Effect of CP, RA (10, 20, 40 mg/kg), and NER (400 mg/kg) on oxidative stress markers in cardiac tissue of Swiss albino mice
CP 200 administration caused a significant reduction in (CAT, SOD, GSH), along with an elevation in nitrite and MDA levels in cardiac tissue. Treatment with RA (20 and 40 mg/kg) along with NER (400 mg/kg) significantly restored antioxidant enzyme activities and normalized nitrite and MDA levels. The perse group showed no significant differences. Results are expressed as mean ± SEM (n = 6). Statistical analysis was performed using one-way ANOVA followed by Tukey's test, where ###P<0.001 significant vs control; *P<0.05, **P<0.01, ***P<0.001 significant vs CP 200; and ns (P>0.05) indicated non-significant changes vs CP 200. CP: cyclophosphamide; RA: rotundic acid; NER: nerolidol; SOD: superoxide dismutase; CAT: Catalase; GSH: glutathione; MDA: malondialdehyde; TBARS: thio barbituric acid reactive substances

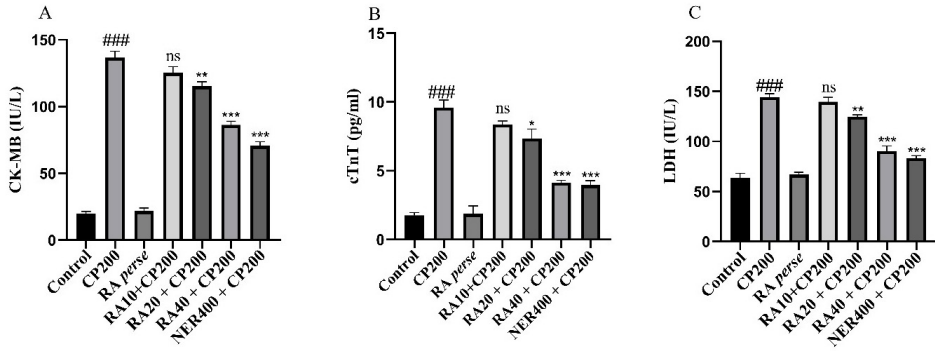

Figure 5. Effect of CP 200, RA (10, 20, 40 mg/kg), and NER (400 mg/kg) on cardiac injury markers (cTnT, CK-MB, and LDH) in Swiss albino mice
CP 200 administration significantly increased cardiac tissues' cTnT, CK-MB, and LDH levels. Treatment with RA (20 and 40 mg/kg) along with NER (400 mg/kg) significantly normalized cTnT, CK-MB, and LDH. The perse group showed no significant differences. Results are expressed as mean ± SEM (n = 6). Statistical analysis was performed using one-way ANOVA followed by Tukey's test, where ###P<0.001 significant vs control; *P<0.05, **P<0.01, ***P<0.001 significant vs CP 200; and ns (P>0.05) indicated non-significant changes vs CP 200. CP: cyclophosphamide; RA: rotundic acid; NER: nerolidol; cTnT: cardiac troponin T; CK-MB: Creatinine kinase myocardial band; LDH: lactate dehydrogenase

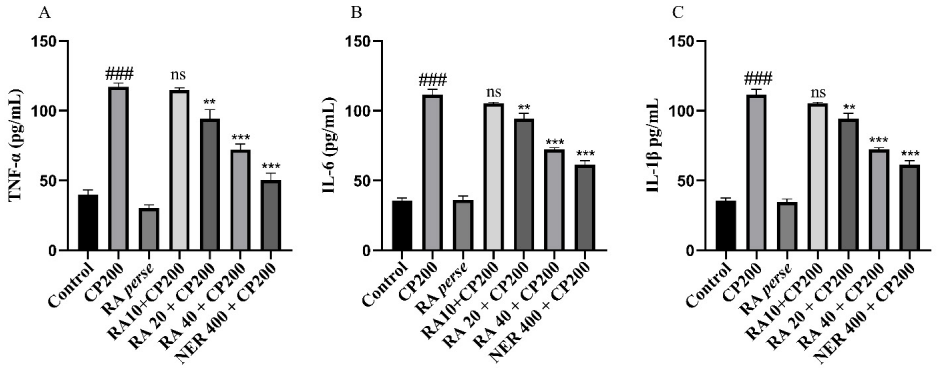

Figure 6. Effect of CP 200, RA (10, 20, 40 mg/kg), and NER (400 mg/kg) on inflammatory markers (TNF-α, IL-6 &, IL-1β) of cardiac tissue in Swiss albino mice
Mice intoxicated with CP 200 displayed marked increase in IL-6, IL-1β, and TNF-α levels in cardiac tissue. Treatment with RA 20, RA 40, and NER 400 significantly reversed them towards normal. The perse group did not show any significant changes. The outcomes are expressed as mean ± SEM (n = 6). Statistical analysis was performed using one-way ANOVA followed by Tukey's test, where ###P<0.001 significant vs control; **P<0.01, ***P<0.001 significant vs CP 200; and ns (P>0.05) showed non-significant changes vs CP 200. CP: cyclophosphamide; RA: rotundic acid; NER: nerolidol; cTnT, TNF-α: Tumor necrosis factor alpha; IL-6: Interleukin 6; IL-1β: Interleukin 1 beta

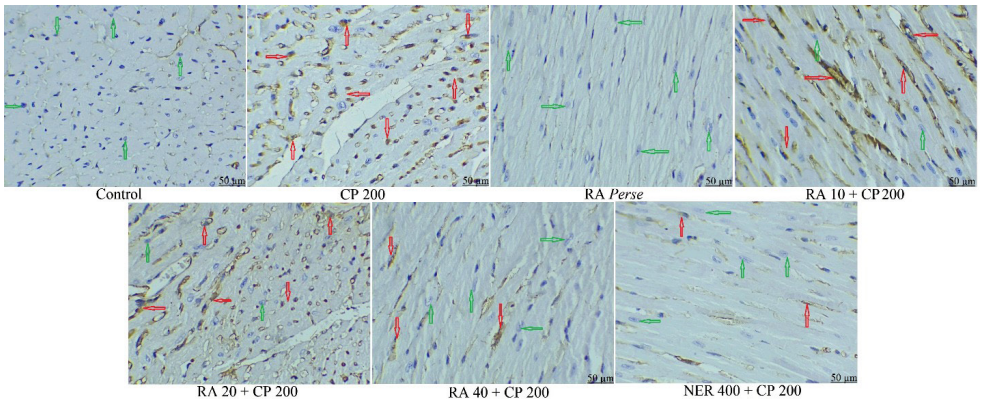

Figure 7. Showing the effects of RA, NER, and CP 200 on immunohistochemical evaluation of NF-κB expression (Scale bar 50 µm) in cardiac tissue of Swiss albino mice
The control group showed minimal expression in NF-κB level (Green arrow), and CP 200 (Toxic group) showed a significant increase in NF-κB expression (red arrow), when compared to the control group. The RA per se group showed similar NF-κB expression as that of the control (Green arrow). The RA10 group showed a non-significant reduction of NF-κB expression compared to the toxic group. The RA 20 group showed moderate reduction of NF-κB expression as compared to the toxic group. The RA 40 and NER 400 groups showed significant reduction of NF-κB expression compared to the toxic group. CP: cyclophosphamide; RA: rotundic acid; NER: nerolidol; IHC: immunohistochemistry; NF-κB: nuclear factor kappa-light-chain-enhancer of activated B cells

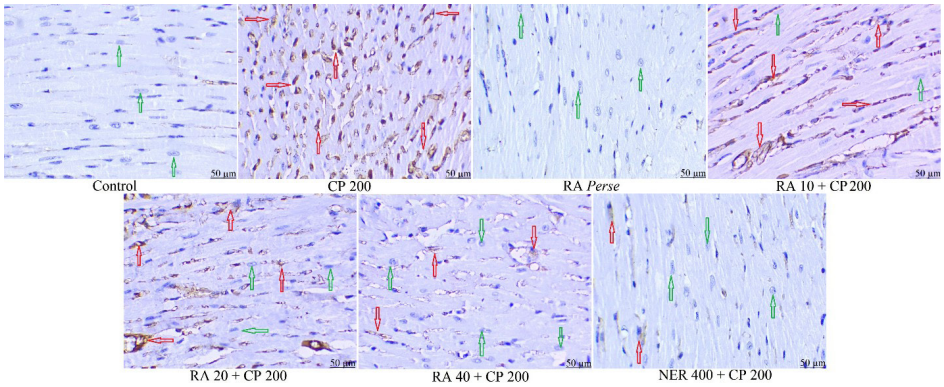

Figure 8. Representative IHC images showing CP200-mediated elevation of cleaved caspase-3 expression in cardiac tissue of Swiss albino mice (scale bar: 50 µm)
The control group showed minimal expression of cleaved caspase-3 level (Green arrow), CP 200 (Toxic group) showed significant increase in cleaved caspase-3 expression (red arrow) when compared with the control group. RA perse group showed similar cleaved caspase-3 expression as that of the control (Green arrow). The RA10 group exhibited a non-significant reduction of cleaved caspase-3 expression as compared to the toxic group. The RA 20 group showed moderate reduction of cleaved caspase-3 expression as compared to the toxic group. The RA 40 and NER 400 groups showed significant reduction of cleaved caspase-3 expression as compared to the toxic group. CP: cyclophosphamide; RA: rotundic acid; NER: nerolidol; IHC: immunohistochemistry

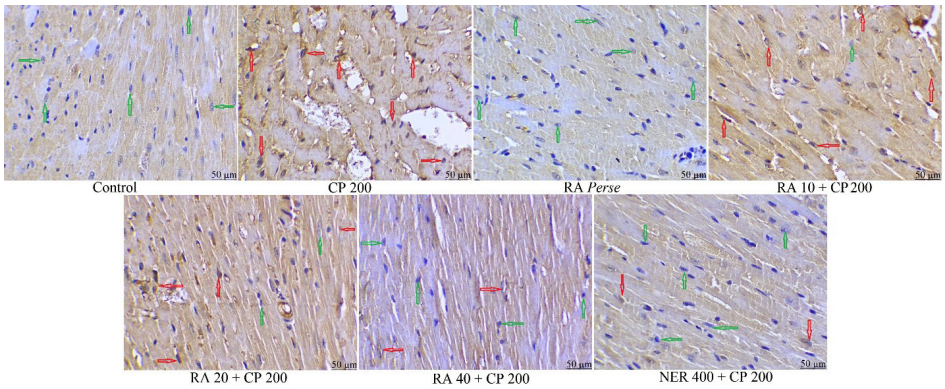

Figure 9. Illustrative IHC images showing CP 200-mediated elevation of TLR-4 expression in cardiac tissue of Swiss albino mice (scale bar: 50 µm)
The Control group exhibited minimal expression in TLR-4 level (Green arrow), and CP 200 (Toxic group) showed a significant increase in TLR-4 expression (red arrow) when compared with the control group. The RA perse group showed similar TLR-4 expressions as that of the control (Green arrow). The RA10 group demonstrated a non-significant reduction in TLR-4 expression as compared to the toxic group. The RA 20 group displayed moderate reduction of TLR-4 expression as compared to the toxic group. The RA 40 and NER 400 groups showed significant reduction of TLR-4 expression as compared to the toxic group. CP: cyclophosphamide; RA: rotundic acid; NER: nerolidol; IHC: immunohistochemistry; TLR4: Toll like receptor 4

Estimation of cardiac fibrosis by Masson's trichrome (MT) staining

MT staining showed no fibrosis in the control. CP 200 caused fibrosis in the cardiac tissue, as shown in Figure 10 by red arrows. Treatment with RA 20, 40, and NER 400 significantly prevented fibrosis, whereas RA 10 showed less reversal of fibrosis. *Perse* group showed no fibrosis (Figures 10 and 11).

Histopathology (H & E staining)

The CP 200 group has shown cellular disintegration, vacuolation, pyknosis, and fibrotic changes in

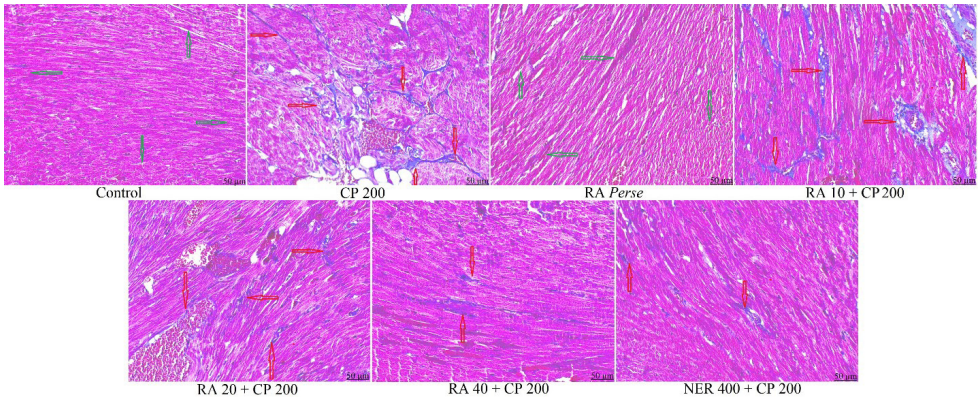

Figure 10. Showing the effects of RA, NER, and CP 200 on the estimation of Masson's Trichrome staining (Scale bar 50 µm) in cardiac tissue of Swiss albino mice
Green arrows represent restored cardiac tissue, and red arrows represent MT staining. The CP 200 group showed cardiac fibrosis as indicated by the (blue colored area). Treatment with RA 20, 40, and NER 400 reversed these fibrotic changes. CP: cyclophosphamide; RA: rotundic acid; NER: nerolidol; MT: Masson's trichrome staining

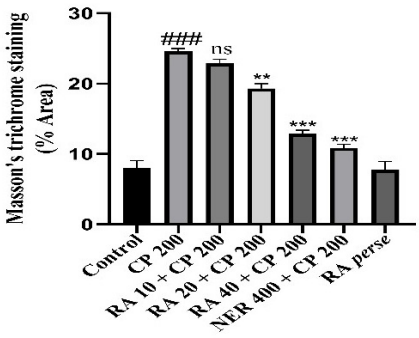

Figure 11. Semi-quantitative examination of MT-stained sections
The data were assessed using one-way (ANOVA) with Tukey's Test. Here, ### (P<0.001) denotes significance versus normal control, ** P<0.01, *** P<0.001 denotes significance v/s CP 200; and ns denotes non-significant v/s CP 200. CP: cyclophosphamide; RA: rotundic acid; NER: nerolidol; MT: Masson's trichrome staining

histopathological visualization. The RA10 group showed a similar pattern of toxicity as compared to the CP group. The RA 20 group showed mild cardiac damage as compared to the CP 200 group. RA 40 and NER 400 groups reversed these damages to normal. RA *perse* has shown normal arrangement of cardiac tissue as that of control group (Figure 13).

Discussion

Cyclophosphamide (CP) is a widely used drug for cancer, autoimmune illness, and bone marrow transplantation (33). The efficacy of CP in preventing tumor development is dependent on its dosage. Higher CP dose may cause significant heart damage (33). Cardiotoxicity due to CP has been described as a problem in several clinical and experimental investigations. The current study aimed to

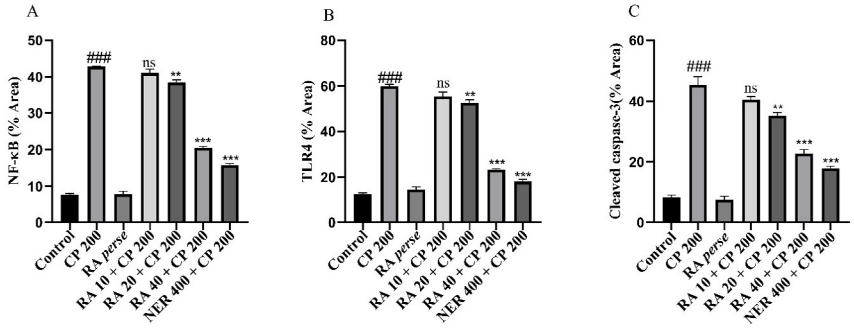

Figure12. Semi-quantitative examination of various markers [A] NF-κB, [B] TLR-4, and [C]
Cleaved caspase-3, in cardiac tissue of Swiss albino mice by using Immunohistochemistry. Data was evaluated by using one-way (ANOVA) with Tukey's method, and the results are shown as mean ± SEM. ###(P<0.001) reveals significance versus control; **P<0.01,***P<0.001 indicate significance v/s CP; and ns indicates non-significant against CP 200. CP: cyclophosphamide; RA: rotundic acid; NER: nerolidol; NF-κB: nuclear factor kappa-light-chain-enhancer of activated B cells; TLR4: Toll like receptor 4

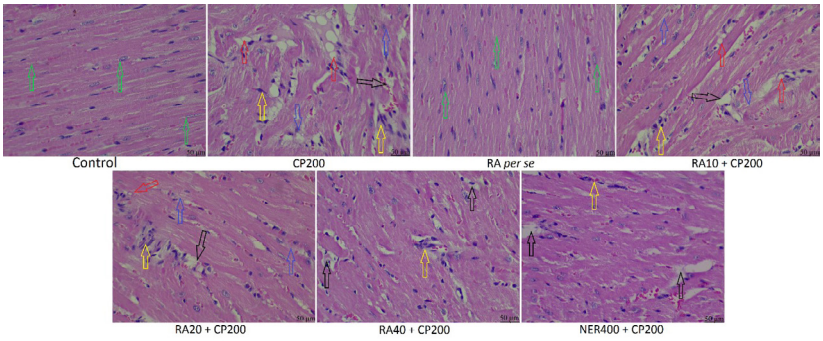

Figure 13. Histopathological assessment of cardiac tissue by H&E staining in Swiss albino mice experimental groups (scale bar: 50 µm)
CP 200 mice showed cardiac histological changes characterized by cellular disintegration (black arrow), pyknotic nuclei (yellow arrow), vacuolization (red arrow), and fibrosis (blue arrow). Treatment with RA 20, 40, and NER 400 reversed these changes, whereas RA 10 was found ineffective. CP: cyclophosphamide; RA: rotundic acid; nerolidol, H&E: Hematoxylin & Eosin

induce cardiotoxicity using CP at 200 mg/kg and to assess the potential effect of RA at different dosages.

Cardiotoxicity is characterized by increased oxidative stress, excessive calcium buildup, reactive nitrogen species, and oxygen species (34). SOD, GSH, and CAT, which regulate superoxide and peroxide ions, protect healthy cardiomyocytes from oxidative stress. If decreased, then it becomes the most important element in the development of cardiovascular diseases (35). Lipid peroxidation products that cause structural and functional heart damage include MDA (36, 37). The primary indicators used to evaluate oxidative stress are GSH SOD, CAT, and TBARS. GSH, SOD, and CAT levels fall under stress conditions, whereas TBARS increase during lipid peroxidation. We found that CP 200 increased lipid peroxidation and decreased GSH, CAT, and SOD levels, suggesting the onset of oxidative stress that led to cardiotoxicity. Treatment with RA 20, 40, and NER 400 mg/kg reversed and restored these parameters to normal, demonstrating cardio-protection. However, treatment with RA 10 mg/kg showed no significant effects on these markers (Figure 4 A-D). The present findings are consistent with the earlier report (16). NO and superoxide radicals produce peroxynitrite, which hinders a range of mitochondrial enzymes that subsequently result in nitrative stress, which further causes heart failure, hypertension, and angina pectoris. It also promotes apoptosis and myocardial inflammation (38–40). Cardiac dysfunction was also evident in increased inflammatory responses, driven by TNF-α and NO production, which were stimulated by NF-κB activation (41). Our findings demonstrated that CP 200 mg/kg markedly increased the nitrite levels, leading to enhanced nitrative stress, whereas RA 20, 40 mg/kg and NER 400 mg/kg treatment significantly reduced this level (Figure 4E), which is consistent with the previous report (42). RA 10 mg/kg, however, showed no significant changes in these parameters.

Cardiac troponin T (cTnT), CK-MB, and LDH are released because of myocardial membrane damage caused by oxidative stress. Thus, any medication that decreases the concentration of these indicators towards normal manifests a cardio-protective effect (43). In our study, rotundic acid exhibited cardioprotection, as evidenced by significant reductions in cTnT, CK-MB, and LDH levels, which were markedly elevated by CP (200 mg/kg) administration. Treatment with RA (20, 40 mg/kg) and NER (400 mg/kg) restored these markers to near normal levels; however, RA (10 mg/kg) was found ineffective in reversing these changes (Figure 5 A-C). These findings therefore suggest improved membrane integrity and cardioprotection, aligning well with previously reported results (44).

NF-κB is considered a prominent beneficial target for cardiotoxic effects due to its pivotal involvement in heart dysfunction by causing a rise in the levels of cytokines, namely IL-1β, TNF-α, and IL-6. Cardiac hypertrophy and fibrosis in animals exhibit increased oxidative damage and inflammation due to elevated NF-κB (45). Previous research suggested that CP-induced cardiac damage is associated with cytokine production, which is controlled by NF-κB (46). During exposure to cardio-toxic medications such as doxorubicin, CP, and isoproterenol, there was a considerable increase in IL1β, TNF-α, and IL-6. These cytokines trigger multiple inflammatory processes, leading to heart cell death (47). Our studies also showed that treatment with CP 200 mg/kg significantly elevated cytokine levels, including IL-6, TNF-α, and IL-1β, suggesting inflammation in the heart muscles, and treatment with RA at doses of 20, 40 mg/kg, and NER at 400 mg/kg significantly lowered these inflammatory cytokines towards normal and demonstrated cardioprotection (Figure 6). The present findings are consistent with the earlier reports (3).

Another manifestation of cardiotoxicity is apoptosis, and one key indicator of apoptosis is elevated cleaved caspase 3. Cleaved caspase-3, an executioner caspase, is an important mediator of apoptosis in mammalian cells, leading to DNA fragmentation, protein degradation, and chromatin condensation (48). Our investigation showed that CP 200 treatment increased cleaved caspase-3 expression. When we treated animals with RA 20, 40, and NER 400 mg/kg, we found a considerable reduction in caspase 3, confirming anti-apoptotic action, which is consistent with the previous report (49).

Toll-like receptor 4 (TLR4), a crucial receptor of the innate immune system, detects both endogenous and exogenous stimuli and triggers inflammatory responses in various organs, including the heart. Upon ligand binding, TLR4 forms a complex with Myeloid differentiation protein 2 (MD2) and activates the myeloid differentiation primary response 88 (MyD88)-dependent signaling pathways, which promote NF-κB phosphorylation and enhance the expression of pro-inflammatory cytokines, thereby contributing to cardiac inflammation (50). Activation of TLR-4 promotes the stimulation of NF-κB and mitogen-activated protein kinases (MAPK) signaling pathways. (51). Our investigation also revealed that CP at 200 mg/kg, *IP* resulted in an increased expression of TLR4 and NF-κB. RA 20, 40, and NER 400 decreased their expression to normal. Therefore, this result is similar to the previous studies that showed the essential role of TLR4 in the progression of CP-induced cardiotoxicity (16).

Gravimetric parameters such as HW (heart weight) and BW (body weight) are affected by CP 200 mg/kg, resulting in an increase in HW and a decrease in BW for all animals. This indicates that when mice were exposed to toxicity by CP treatment, there was necrosis in the cardiac tissue and infiltration of inflammatory cells in the injured region of the heart, leading to an enlarged heart or tissue edema (52). The HW/BW ratio is also an excellent gravimetric parameter for detecting edema and congestion after myocardial infarction. The increased ratio indicates elevated cardiac hypertrophy, a response aimed at maintaining adequate heart output. In addition, it may be caused by increased protein content, cellular infiltration, and water accumulation in edematous intramuscular regions. Our investigation revealed that the HW/BW ratio was elevated in CP 200 toxicity, which was reduced by the administration of RA 20, 40 mg/kg, and NER 400 mg/kg (Table 2). Our result is consistent with the previous findings (53).

The MT-staining technique is applied to assess fibrosis in cardiac tissue, specifically identifying collagen-rich sections that are non-perivascular or perivascular. In these fibrotic areas, the staining results in a blue coloration for the collagen, a pink and red coloration for the cytoplasm, and a deep-brown and black coloration for the nucleus (54). Based on the staining technique used, our research demonstrated a substantial increase in the fibrotic region of the CP 200-treated group. RA 20, 40, and NER 400 mg/kg extensively decreased the fibrotic region towards normal and exhibited an anti-fibrotic action against CP 200 (Figure

10). This result thus aligns with the prior research and demonstrates the protective effect of our test drugs (55).

Hematoxylin and eosin (H&E) staining is a crucial method in histopathology for analyzing cellular & structural alterations in cardiac muscle. Our investigation found that animals treated with CP 200 exhibited pyknosis or myofibrillar disintegration, as well as vacuolization in some regions of the heart muscle. Treatment with RA 20, 40, and NER 400 mg/kg effectively decreased these alterations to normal and showed protection against CP-induced tissue injury, which is consistent with the previous study (56). (Figure 13). Thus, considering all the parameters studied, we can say that RA significantly reduced the CP-induced toxicity in mice and may be used as an adjuvant in cancer therapy. However, the limitation of this study is that the cardioprotective activity of rotundic acid was evaluated against CP using normal (non-tumor-bearing) mice. So, how it will behave in a cancer model is not clear. Hence, further investigation in a tumor-bearing model is required to confirm its efficacy and potential applicability as an adjuvant under cancer-related conditions.

Conclusion

Our study revealed that administration of CP at 200 mg/kg resulted in a significant increase in oxidative and nitrative stress, cardiac inflammation, apoptosis, fibrosis, tissue damage, and the HW/BW ratio. Compared with NER 400 mg/kg, RA 40 mg/kg dramatically reduced cardiotoxic effects and showed stronger cardioprotective benefits. RA at 10 mg/kg did not provide significant protection. Thus, we can conclude that RA is a potential cardioprotective agent that reduces CP-induced cardiotoxicity and, if given together with CP in a tumor-bearing model, may open an avenue for adjuvant therapies. However, further investigations employing tumor-bearing animal models are required to evaluate the efficacy and elucidate the precise role of rotundic acid under pathophysiological conditions.

Acknowledgment

We are thankful to Jamia Hamdard, India, for providing the necessary facilities to perform the experimental work.

Funding

This research did not receive any specific grant from funding agencies in the public, commercial, or not-for-profit sectors.

Authors' Contributions

M M performed experiments, compiled data, and prepared the draft. MSB performed *in silico* experiments. D V co-supervised and helped draft the manuscript. SE H conceptualized and supervised the entire project.

Conflicts of Interest

There are no conflicts of interest.

Declaration

This manuscript was not written using any AI tools.

References

1. Ahlmann M and Hempel G. The effect of cyclophosphamide on the immune system: Implications for clinical cancer therapy. Cancer Chemother Pharmacol 2016; 78:661–671.
2. Iqubal A, Wasim Mohd, Ashraf Mohd, Najmi AK, Syed MA, Ali J, *et al.* Natural bioactive as a potential therapeutic approach for the management of cyclophosphamide-induced cardiotoxicity Curr Top Med Chem 2021; 21:2647–2670.
3. Iqubal A, Sharma S, Ansari MA, Najmi AK, Syed MA, Ali J, *et al.* Nerolidol attenuates cyclophosphamide-induced cardiac inflammation, apoptosis and fibrosis in Swiss albino mice. Eur J Pharmacol 2019; 863:172666.
4. Singh RK, Kumar S, Prasad DN, Bhardwaj TR. Therapeutic journery of nitrogen mustard as alkylating anticancer agents: Historic to future perspectives. Eur J Med Chem 2018; 151:401–433.
5. Zorov DB, Juhaszova M, Sollott SJ. Mitochondrial reactive oxygen species (ROS) and ROS-induced ROS release. Physiol Rev 2014; 94:909–950.
6. Angsutararux P, Luanpitpong S, Issaragrisil S. Chemotherapy-induced cardiotoxicity: overview of the roles of oxidative stress. Oxid Med Cell Longev 2015; 2015:1–13.
7. Wasim M, Ali SM, and Haque SE. Verbenone prevents cyclophosphamide-induced oxidative stress, inflammation, fibrosis, and cellular changes in the kidneys of Swiss albino mice by targeting NF-κB/TGF-β signaling pathways. Iran J Basic Med Sci 2025; 28 :1119–1128.
8. Yan Z, Su M, Pan W, Su W, and Wang Y. A simple method for extraction and purification of pedunculoside from the dried barks of *Ilex rotunda* and its inhibitory effect on pancreatic lipase in vitro. Sep Sci Technol 2017; 52:2878–2887.
9. Bhuia MdS, Chowdhury R, Sonia FA, Biswas S, Ferdous J, El-Nashar HAS, *et al.* Efficacy of rotundic acid and Its derivatives as promising natural anticancer triterpenoids: A literature-based study. Chem Biodivers 2024; 21:e202301492.
10. Li X, Yuan R, Wang Q, Han S, Liu Z, Xu Q, *et al.* Rotundic acid reduces LPS induced acute lung injury in vitro and in vivo through regulating TLR4 dimer. Phytother Res 2021; 35:4485–4498.
11. Roy G, Guan S, Liu H, and Zhang L. Rotundic acid induces DNA damage and cell death in hepatocellular carcinoma through AKT/mTOR and MAPK pathways. Front Oncol 2019; 9:545-560.
12. Shi X-Y, Zheng X-M, Liu H-J, Han X, Zhang L, Hu B, *et al.* Rotundic acid improves nonalcoholic steatohepatitis in mice by regulating glycolysis and the TLR4/AP1 signaling pathway. Lipids Health Dis 2023; 22:214-231.
13. Chan W-K, Tan L, Chan K-G, Lee L-H, and Goh B-H. Nerolidol: A sesquiterpene alcohol with multi-faceted pharmacological and biological activities. Molecules 2016; 21:529-568.
14. Arunachalam S, Nagoor Meeran MF, Azimullah S, Sharma C, Goyal SN, Ojha S. Nerolidol attenuates oxidative stress, inflammation, and apoptosis by modulating Nrf2/MAPK signaling pathways in doxorubicin-induced acute cardiotoxicity in rats. Antioxidants 2021; 10:984-997.
15. Iqubal A, Syed MA, Ali J, Najmi AK, Haque MM, Haque SE. Nerolidol protects the liver against cyclophosphamide-induced hepatic inflammation, apoptosis, and fibrosis via modulation of Nrf2, NF-κB p65, and caspase-3 signaling molecules in Swiss albino mice. BioFactors 2020; 46:963–973.
16. Akram W, Najmi AK, Alam MM, and Haque SE. Levocabastine ameliorates cyclophosphamide-induced cardiotoxicity in Swiss albino mice: Targeting TLR4/NF-κB/NLRP3 signaling pathway. Toxicol Appl Pharmacol 2024; 483:116838.
17. Liu H-J, Cao S-T, Wen B-Y, Han X, Li Y, Li S, *et al.* Rotundic acid ameliorates non-alcoholic steatohepatitis via SREBP-1c/SCD1 signaling pathway and modulating gut microbiota. Int Immunopharmacol 2021; 99:108065.
18. Yan Z, Wu H, Yao H, Pan W, Su M, Chen T, *et al.* Rotundic acid protects against metabolic disturbance and improves gut microbiota in type 2 diabetes rats. Nutrients 2019; 12:67-83.
19. Schrödinger L, & DW. PyMOL. http://www.pymol.org/pymol. 2020.
20. Guex N, Peitsch MC. SWISS-MODEL and the Swiss-Pdb Viewer: An environment for comparative protein modeling. Electrophoresis 1997; 18:2714–2723.

21. Trott O and Olson AJ. AutoDock Vina: Improving the speed and accuracy of docking with a new scoring function, efficient optimization, and multithreading. J Comput Chem 2010; 31:455–461.
22. Morris GM, Huey R, Lindstrom W, Sanner MF, Belew RK, Goodsell DS, *et al.* Auto dock4 and autodockTools4: automated docking with selective receptor flexibility. J Comput Chem 2009; 30:2785–2791.
23. Iqbal A, Fatima Z, Ali F, Zafar F, Bibi S, Sajid M, *et al. In silico* screening of phytochemicals targeting the NF-κB pathway: A novel approach for pancreatic cancer drug discovery. J Comput Biophys Chem 2026; 25:769–785.
24. Iqbal A, Sabir AN, Ali F, Abdelkrim G, Bibi S, Sajid M, *et al.* Computational design and immunoinformatic analysis of a multi-epitope vaccine targeting zika virus EDIII protein. J Comput Biophys Chem 2026; 25:965–981.
25. Islam MdT, Aktaruzzaman Md, Barai C, Rafi FI, Hasan AR, Tasnim T, *et al. In silico* screening of naturally derived dietary compounds as potential butyrylcholinesterase inhibitors for alzheimer's disease treatment. Sci Rep 2025; 15:17134-171155.
26. MARKLUND S and MARKLUND G. Involvement of the superoxide anion radical in the autoxidation of pyrogallol and a convenient assay for superoxide dismutase. Eur J Biochem 1974; 47:469–474.
27. Claiborne A. Handbook of methods for oxygen radical research. Florida: CRC Press, Boca Raton 1985; 283–284.
28. Sedlak J and Lindsay RH. Estimation of total, protein-bound, and nonprotein sulfhydryl groups in tissue with Ellman's reagent. Anal Biochem 1968; 25:192–205.
29. Ohkawa H, Ohishi N, and Yagi K. Assay for lipid peroxides in animal tissues by thiobarbituric acid reaction. Anal Biochem 1979; 95:351–358.
30. Richa R, Yadawa AK, and Chaturvedi CM. Hyperglycemia and high nitric oxide level induced oxidative stress in the brain and molecular alteration in the neurons and glial cells of laboratory mouse, Mus musculus. Neurochem Int 2017; 104:64–79.
31. Sharma S, Khan V, Dhyani N, Najmi A, and Haque S. Icariin attenuates isoproterenol-induced cardiac toxicity in Wistar rats via modulating cGMP level and NF-κB signaling cascade. Hum Exp Toxicol 2020; 39:117–126.
32. Sharma S, Khan V, Najmi A, Alam O, and Haque S. Prophylactic treatment with icariin prevents isoproterenol-induced myocardial oxidative stress via nuclear Factor-Like 2 activation. Pharmacogn Mag 2018; 14:227-236.
33. Emadi A, Jones RJ, and Brodsky RA. Cyclophosphamide and cancer: Golden anniversary. Nat Rev Clin Oncol 2009; 6:638–647.
34. Angsutararux P, Luanpitpong S, and Issaragrisil S. Chemotherapy-induced cardiotoxicity: Overview of the roles of oxidative Stress. Oxid Med Cell Longev 2015; 2015:1–13.
35. Asiri YA. Probucol attenuates cyclophosphamide-induced oxidative apoptosis, p53 and bax signal expression in rat cardiac tissues. Oxid Med Cell Longev 2010; 3:308–316.
36. Tapio S. Pathology and biology of radiation-induced cardiac disease. J Radiat Res 2016; 57:439–448.
37. Ping Z, Peng Y, Lang H, Xinyong C, Zhiyi Z, Xiaocheng W, *et al.* Oxidative stress in radiation-induced cardiotoxicity. Oxid Med Cell Longev 2020; 2020:1–15.
38. Radi R, Cassina A, Hodara R, Quijano C, and Castro L. Peroxynitrite reactions and formation in mitochondria. Free Radic Biol Med 2002; 33:1451–1464.
39. Nickola MW, Wold LE, Colligan PB, Wang G-J, Samson WK, and Ren J. Leptin attenuates cardiac contraction in rat ventricular myocytes. Hypertension 2000; 36:501–505.
40. Nakazawa H, Chang K, Shinozaki S, Yasukawa T, Ishimaru K, Yasuhara S, *et al.* iNOS as a driver of inflammation and apoptosis in mouse skeletal muscle after burn injury: Possible involvement of Sirt1 S-nitrosylation-mediated acetylation of p65 NF-κB and p53. PLoS One 2017; 12:e0170391.
41. El-Agamy DS, Elkablawy MA, Abo-Haded HM. Modulation of cyclophosphamide-induced cardiotoxicity by methyl palmitate. Cancer Chemother Pharmacol 2017; 79:399–409.
42. El kiki SM, Omran MM, Mansour HH, and Hasan HF. Metformin and/or low dose radiation reduces cardiotoxicity and apoptosis induced by cyclophosphamide through SIRT-1/SOD and BAX/Bcl-2 pathways in rats. Mol Biol Rep 2020; 47:5115–5126.
43. Noszczyk-Nowak A. NT-pro-BNP and troponin I as predictors of mortality in dogs with heart failure. Pol J Vet Sci 2011; 14:551–556.
44. Gore PR, Prajapati CP, Mahajan UB, Goyal SN, Belemkar S, Ojha S, *et al.* Protective effect of thymoquinone against cyclophosphamide-induced hemorrhagic cystitis through inhibiting DNA damage and upregulation of Nrf2 expression. Int J Biol Sci 2016; 12:944–953.
45. Zhao L, Wu D, Sang M, Xu Y, Liu Z, and Wu Q. Stachydrine ameliorates isoproterenol-induced cardiac hypertrophy and fibrosis by suppressing inflammation and oxidative stress through inhibiting NF-κB and JAK/STAT signaling pathways in rats. Int Immunopharmacol 2017; 48:102–109.
46. Liu Y, Tan D, Shi L, Liu X, Zhang Y, Tong C, *et al.* Blueberry anthocyanins-enriched extracts attenuate cyclophosphamide-induced cardiac injury. PLoS One 2015; 10:e0127813.
47. Capone F, Guerriero E, Sorice A, Colonna G, Storti G, Pagliuca J, *et al.* Synergistic antitumor effect of doxorubicin and tacrolimus (FK506) on hepatocellular carcinoma cell lines. Sci World J 2014; 2014:1–9.
48. Wanas H, El-Shabrawy M, Mishriki A, Attia H, Emam M, Aboulhoda BE. Nebivolol protects against cyclophosphamide-induced nephrotoxicity through modulation of oxidative stress, inflammation, and apoptosis. Clin Exp Pharmacol Physiol 2021; 48:811–819.
49. Asiri YA. Probucol Attenuates cyclophosphamide-induced oxidative apoptosis, p53 and bax signal expression in rat cardiac issues. Oxid Med Cell Longev 2010; 3:308–316.
50. Sumneang N, Tanajak P, and Oo TT. Toll-like receptor 4 inflammatory perspective on doxorubicin-induced cardiotoxicity. Molecules 2023; 28:4294-4305.
51. Kawasaki T and Kawai T. Toll-like receptor signaling pathways. Front Immunol 2014; 25:461-468.
52. Motawi TMK, Sadik NAH, and Refaat A. Cytoprotective effects of DL-alpha-lipoic acid or squalene on cyclophosphamide-induced oxidative injury: An experimental study on rat myocardium, testicles and urinary bladder. Food Chem Toxicol 2010; 48:2326–2336.
53. Abdulla SK, Rashid BM, Hamaamin KS, Mahmood NN, Marouf BH, and Othman HH. Cardioprotective effect of zofenopril, thymoquinone and their combination in cyclophosphamide-induced cardiotoxicity in rats. Hum Exp Toxicol 2025; 44: 09603271251376594.
54. Nakada Y, Canseco DC, Thet S, Abdisalaam S, Asaithamby A, Santos CX, *et al.* Hypoxia induces heart regeneration in adult mice. Nature 2017; 541:222–227.
55. Abd Allah SH, Hussein S, Hasan MM, Deraz RHA, Hussein WF, and Sabik LME. Functional and structural assessment of the effect of human umbilical cord blood mesenchymal stem cells in doxorubicin-induced cardiotoxicity. J Cell Biochem 2017; 118:3119–3129.
56. Zengin T, Tekelioglu Y, Keskin O, Reis Kose GD, Ari NS, Arici T, *et al.* Histological and flow cytometric evaluation of astaxanthin's effects against cyclophosphamide induced heart injury in rats. Drug Chem Toxicol 2025; 48: 1410-1423.